Particle Accelerators, 1992, Vols. 37–38, pp. 269–274
Reprints available directly from the publisher
Photocopying permitted by license only

BEAM BEHAVIOR DUE TO IMAGE FIELDS

P. JUNIOR and A. HARTH

Institut für Angewandte Physik, J. W. Goethe-Universität, Robert-Mayer-Str. 2–4, D-6000, Frankfurt am Main, Germany.

(Received 3 December 1990)

HIF acceleration usually starts with an RFQ driven under strong space-charge conditions. However, fairly little regard has been given to image forces inherent with high beam currents as determined by HIF. The paper explains and demonstrates two-dimensional calculations of beam behavior with respect to image fields, as caused by more or less displaced beams within metallic quadrupole boundaries.

1 POTENTIAL REPRESENTATION

Restricting to two transverse dimensions, we inspect the transverse complex z-plane of Figure 1a, and, using cylindrical coordinates, represent the potential function of the misaligned circular beam as

$$\Phi(z) = F + \sum_{M=0}^{\max} r^M (A_M^z \cos M\varphi + B_M^z \sin M\varphi). \tag{1}$$

For the space charge term F we assume KV[1] distribution inside the beam (Eq. 2a) and logarithmic dependence outside Eq. (2b):

$$F(r, \varphi, r_q, \varphi_q) = -\frac{I}{4\pi\varepsilon_0 v} \begin{cases} \dfrac{r^2 + r_q^2 - 2rr_q \cos(\varphi - \varphi_q)}{R^2} & \text{(2a)} \\ 1 + \ln \dfrac{r^2 + r_q^2 - 2rr_q \cos(\varphi - \varphi_q)}{R^2}, & \text{(2b)} \end{cases}$$

with particle velocity v, beam current I, beam radius R and dielectric constant ε_0.

Thus the regular transition of both expressions is guaranteed on the beam surface. The expansion coefficients $A_M^z B_M^z$ now have to adjust the potential to the boundary conditions implied by the hyperbolic electrodes of Figure 1a. Of course, they depend strongly on the coordinates $r_q \varphi_q$ of the charge center of the beam. Hence the terms 1 and $\ln R^2$ occurring in the outside potential given by Eq. (2b) can be added to the constant A_0, which does not appear in the equations of motion anyway. Determinations of $A_M^z(r_q, \varphi_q)$, $B_M^z(r_{q_2}, \varphi_q)$ are carried out by means of conformal mapping. The complex relation[2]

$$W = \left(\tan \frac{\pi}{4} z^2\right)^{1/2} \tag{3a}$$

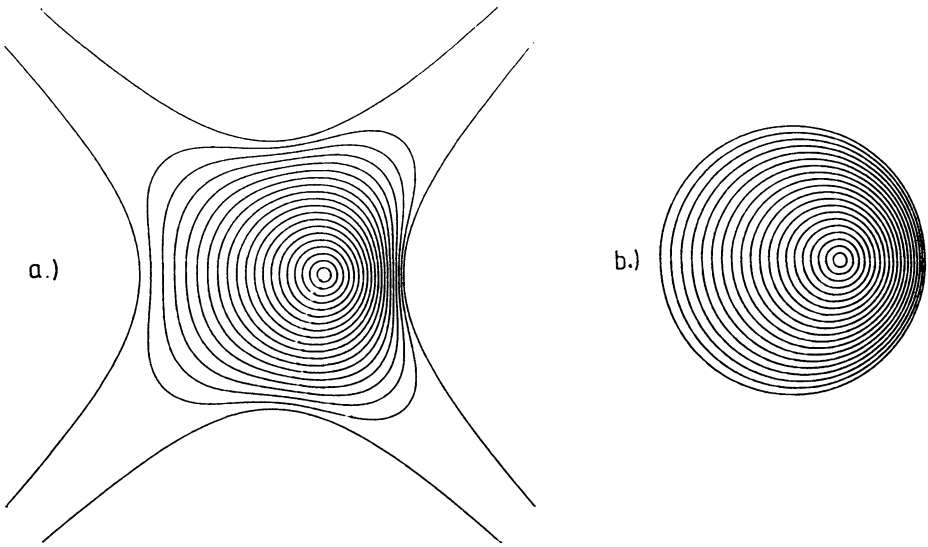

FIGURE 1 Conformal mapping; (a) z-plane, (b) W-plane.

associates the hyperbolas of Figure 1a with the unit circle of Figure 1b. Thus the potential of the misaligned charge center $\rho_q \psi_q$ in W-plane can be determined easily by using an expansion analgous to Eq. (1) and by calculating the coefficients A_M^W and B_M^W—however, with a handier circular boundary in the W plane:

$$A_M^W = \frac{I \cos \psi_q}{4\pi^2 \varepsilon_0 v} \int_0^{2\pi} \ln(1 + \rho_q^2 - 2\rho_q \cos \psi) \cos M\psi \, d\psi. \tag{4}$$

$$B_M^W = \frac{I \sin \psi_q}{4\pi^2 \varepsilon_0 v} \int \ln(1 + \rho_q^2 - 2\rho_q \cos \psi) \cos M\psi \, d\psi$$

(For $M = 0$ 4 should be replaced by 8.)

Accurate numerical displays of both potentials in the W and z planes are established by the transformation

$$z = \left(\frac{2}{\pi i} \ln \frac{1 + iw^2}{1 - iw^2} \right)^{1/2}, \tag{3b}$$

the inverse of Eq. (3a).

Figure 2 shows the dependences of A_M^z and B_M^z on displacement. Curves apply to the quadrupole aperture 1; conversion to realistic apertures and corresponding coefficients A_M, B_M is established by

$$A_M = \frac{A_M^z}{a^M}; \qquad B_M = \frac{B_M^z}{a^M}. \tag{5}$$

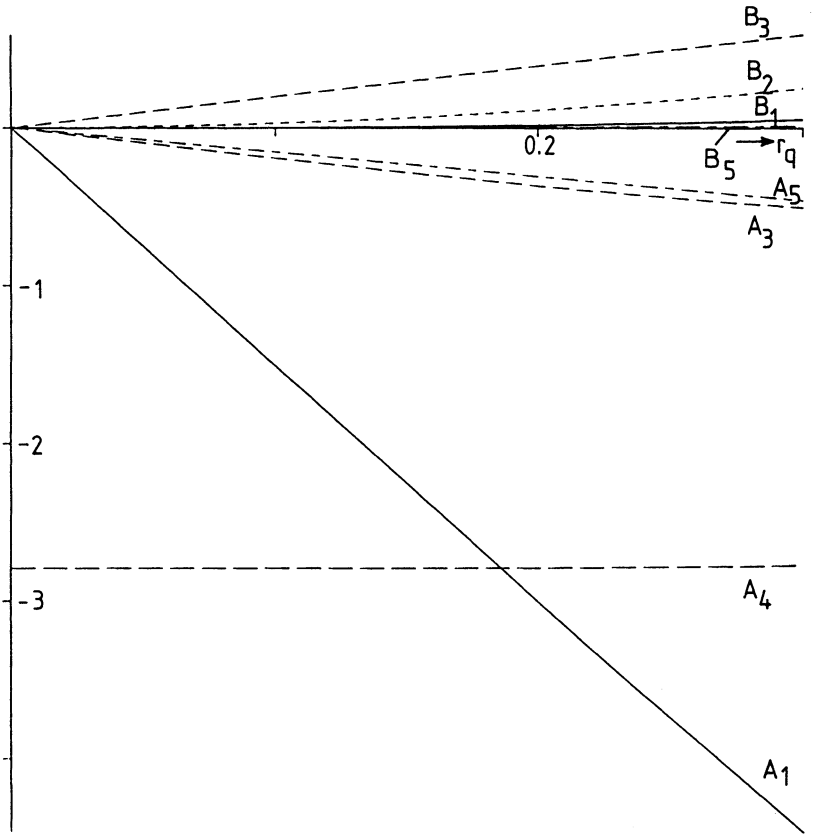

FIGURE 2 $A_M(r_q, \varphi_q = 45°)$, $B_M(r_q, \varphi_q = 45°)$ versus displacement r_q for $M = 1 \ldots 6$.

2 MOTION

In Cartesian coordinates,

$$\frac{d^2x}{d\tau^2} = -\frac{\sigma_0^2}{\pi^2}x + \frac{2eI}{\pi\varepsilon_0 mvw^2}G - \frac{4e}{mw^2}H, \tag{6}$$

$$G = \begin{cases} \dfrac{x - x_q}{R^2} & \text{inside beam} \\ \dfrac{x - x_q}{(x - x_q)^2 + (y - y_q)^2} & \text{outside beam} \end{cases}, \tag{7}$$

$$\begin{aligned} H = {} & A_1 + 2A_2x + 3A_3(x^2 - y^2) + 4A_4(x^3 - 3xy^2) + 5A_5(x^4 - 6x^2y^2 + y^4) \\ & + 6A_6(x^5 - 10x^3y^2 + 5xy^4) + 2B_2y + 6B_3xy + 4B_4(3x^2y - y^3) \\ & + 20B_5(x^3y - xy^3) + 6B_6(5x^4y - 10x^2y^3 + y^5). \end{aligned} \tag{8}$$

For the y component of motion, replace x by y in Eq. (6) but not in Eq. (8). In Eq. (8), replace A_M by B_M and replace B_M by $-A_M$. In Eq. (7), replace $x - x_q$ by $y - y_q$. Further substitutions are $\tau = \omega t/2$ and σ_0^2 in place of the oscillating RFQ field gradient, a common practice in smooth approximation[3]. Using two dimensions requires that the RFQ consist of unmodulated plain electrodes. Computations are based on the Runge–Kutta numerical method. Herein the τ axis is subdivided into short cells and equations are successively integrated for a sufficient number of particles. From cell to cell the displacement of the charge center with respect to the variation of the A_M and B_M terms is permanently determined with conformal mapping as explained in section 1. A further assumption is that the beam should keep its dominant monopole moment throughout, with no multipole moments being excited.

3 NUMERICAL RESULTS

Emphasis was given to the topical acceleration schedule of a high-current RFQ injector for GSI, which is under study in our institute. The parameters are frequency $\omega/2\pi = 27$ MHz, electrode voltage 180 kV, aperture $a = 6.8$ mm, injection of Xe^{1+}_{131} (i.e., Xenon-131 at a $+1$ charge state) ions at an energy of 300 keV, phase advance $\sigma_0 = 25.37°$, and beam current $I = 20$ mA[4,5].

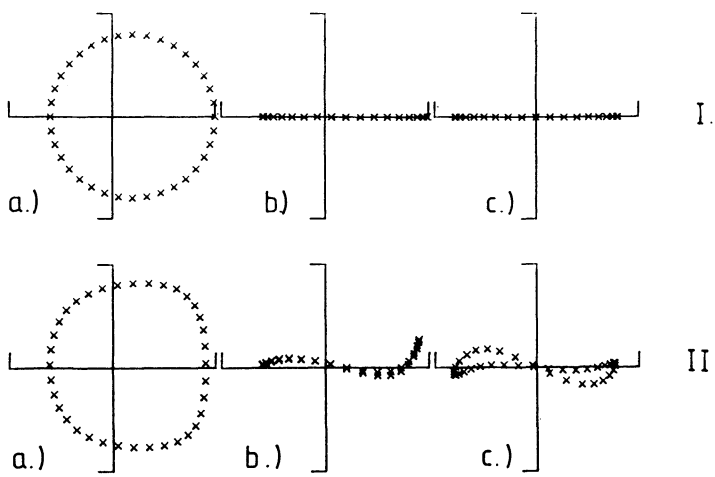

FIGURE 3 Behavior of misaligned beam; (a) x-y-plane, (b) $x - (dx/d\tau)$-plane, (c) y-$(dy/d\tau)$ plane. I. Input state with displacement $r_q = 1.38$ mm. $\varphi_q = 0°$. II. Output state after 70 rf cycles; 27 MHz, 6.8 mm, and 180-kV schedule.

Figure 3 demonstrates the behavior of a displaced beam; there is fairly small evidence of nonlinear image fields. It takes almost 70 rf cycles for the circular beam to lose its roundness. Then, as shown in Figure 4, the aligned beam was investigated. Only the octupole moment A_4 interacts in this case.

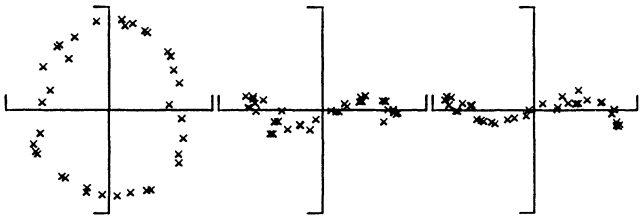

FIGURE 4 Aligned beam of Figure 3.

In order to articulate the effects of image forces, a smaller aperture was chosen and the electrode voltage 97.31 kV was scaled for the same σ_0. Figures 5 and 6 illustrate the greater self-disorganization of the 20 mA beam at 97 kV. In our examples we have chosen initial displacements $\varphi_q = 0$, because in this case nonlinear evidence shows up more distinctly.

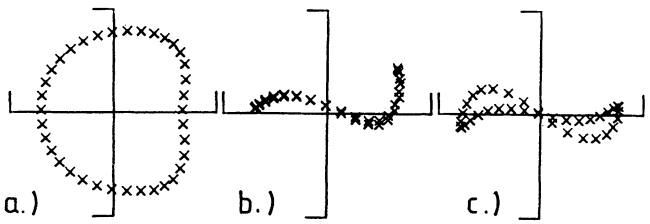

FIGURE 5 Behavior of misaligned beam; (a) x-y-plane, (b) $x - (dx/d\tau)$-plane, (c) $y - (dy/d\tau)$-plane. Output state after 70 rf cycles; 27 MHz, 5 mm, and 97.3-kV schedule.

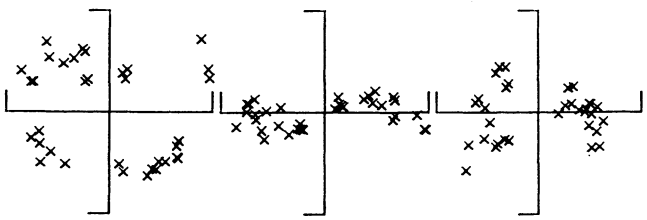

FIGURE 6 Aligned beam of Figure 5.

4 SUMMARY

Calculations show fairly small effects from image forces in our present schedule due to the rather large aperture. Smaller apertures in a high-current RFQ, however, demand thorough consideration.

ACKNOWLEDGEMENTS

The authors are indebted to the Hochschulrechenzentrum of the University of Frankfurt. The RFQ research program is sponsored by the BMFT.

REFERENCES

1. I. M. Kapchinskiy and V. V. Vladimirskiy, Proc. Int. Conf. on High Energy Acc., CERN, Geneva (1959) p. 274.
2. K. Halbach, LBL, seminar lecture, University of Frankfurt, Nov. 17, 1989, Anwendungen von konformen Abbildungsmethoden.
3. P. Junior, *Part. Accel.*, **13** 231 (1983).
4. A. Schempp *et al.*, *Nucl. Instrum. Meth.* A **278** 169 (1989).
5. H. Deitinghoff *et al.*, these Proceedings.